Magnetochemistry of the Tetrahaloferrate(III) Ions. 7. Crystal Structure and Magnetic Ordering in (pyridinium)$_3$Fe$_2$Br$_9$

Carol B. Lowe,[1a] Arthur J. Schultz,[1b] Roey Shaviv,[1a] and Richard L. Carlin*[,1a]

Department of Chemistry, University of Illinois at Chicago, Chicago, Illinois 60680, and IPNS Division, Argonne National Laboratory, Argonne, Illinois 60439

Received October 15, 1993[⊗]

A monoclinic crystal structure was found by X-ray diffraction for bis[pyridinium tetrabromoferrate(III)]–pyridinium bromide. The double salt contains two slightly distorted $[FeBr_4]^-$ tetrahedra, three pyridinium rings, and an uncoordinated halide in each asymmetric unit, as is characteristic of the $A_3Fe_2X_9$ series of compounds. Unit cell parameters, monoclinic space group $P2_1$, are a = 7.656(3) Å, b = 14.237(5) Å, c = 13.725(5) Å, β = 93.42(3)°, and V = 1493(1) Å^3, using Mo Kα radiation (λ = 0.710 69 Å), ρ_{calc} = 2.38 g cm^{-3}, and Z = 2. The tetrahedra are aligned with their 3-fold axes parallel to the crystallographic c axis. Bond lengths (Fe–Br) range from 2.271(9) Å to 2.379(9) Å for the two different slightly distorted tetrahedral units. Magnetic susceptibility studies show that the material orders three-dimensionally at 7.4 ± 0.2 K. The data are compared to a HTS expansion of $1/\chi$ for the $S = {}^5/_2$ three-dimensional Heisenberg model antiferromagnet for a sc lattice with g = 1.98 and J/k_B = –0.43 K. The specific heat measurements indicate two odd-shaped λ features, at 7.3 and 8 K.

Introduction

Since our study of the magnetic interactions in orthorhombic bis[pyridinium tetrachloroferrate(III)]–pyridinium chloride,[2] we became interested in the bromide compound of the same stoichiometry, $(pyH)_3Fe_2Br_9$. Preparation of a compound having this stoichiometry and measurements of the magnetic susceptibility and the optical spectrum for the material were reported previously by Ginsberg and Robin.[3] They proposed that the iron in the compound is present entirely as $[FeBr_4]^-$ ions; however, no confirming crystal structure had been done. Their magnetic susceptibility measurements suggested that a pairwise exchange mechanism between interacting spin $^5/_2$ ions was not operative for this material. However, the data were not compared with those for any other model. This paper presents the preparation, X-ray crystal structure, and low-temperature magnetic characterization of a compound found to be $2[pyH][FeBr_4]\cdot[pyH]Br$. The magnetic susceptibility measurements of this compound do not agree with those of Ginsberg and Robin, although similar preparative methods were used and the chemical analyses given are very similar.

It was anticipated that the compound would be isostructural with the analogous chloride described earlier,[2] but this is not the case. Like the chloride, the molecule is arranged as a double salt with the formulation $2[pyH][FeBr_4]\cdot[pyH]Br$, but it crystallizes in monoclinic symmetry. Several other substances known to contain $[FeBr_4]^-$ are described in ref 4, while the chlorides are discussed in ref 5.

Experimental Section

Preparation of Bis[pyridinium tetrabromoferrate(III)]–Pyridinium Bromide. Crystals were prepared as follows: To a solution of 42.1 g (0.142 mol) of $FeBr_3$ in 130 mL of aqueous HBr (4 M) was added a mixture of 23.3 g (0.294 mol) of pyridine and aqueous HBr (75 mL, 4 M). Filtration to remove insolubles was followed by slow evaporation at room temperature. Crystallization culminated after 19 days. Large, nearly opaque crystals, dark red in powdered form, were then collected by filtration and dried *in vacuo*. Anal. Calc for $C_{15}H_{18}Br_9Fe_2N_3$: C, 16.82; H, 1.69; Br, 67.14; Fe, 10.43; N, 3.92. Found: C, 16.48; H, 1.63; Br, 67.53; Fe, 10.30; N, 3.82.

Table 1. Crystallographic Data for $(pyH)_3Fe_2Br_9$

empirical formula: $C_{15}H_{18}Br_9Fe_2N_3$	ρ_{calc} = 2.38 g cm^{-3}
fw 1071	cryst dimens: 0.14 × 0.24 × 0.235 mm^3
space group $P2_1$ (No. 4)	λ(Mo Kα) = 0.710 69 Å
a = 7.656(3) Å	μ = 137.2 cm^{-1}
b = 14.237(5) Å	θ–2θ scans
c = 13.725(5) Å	$0 \le h \le 9$; $0 \le k \le 16$; $-17 \le l \le 16$
β = 93.42(3)°	no. of unique refls measd: 2761
V = 1493(1) Å^3	no. of refls in final ls, $F_o \ge 3\sigma(F_o)$: 1785
Z = 2	$R(F_o)^a$ = 0.112
T = 22 °C	$R_w(F_o)^b$ = 0.074
	GOF[c] = 2.39

$^a R(F_o) = \sum||F_o| - |F_c||/\sum|F_o|$. $^b R_w(F_o) = (\sum w(|F_o| - |F_c|)^2/\sum|F_o|^2)^{1/2}$. ^{c} GOF = $\sum w(|F_o| - |F_c|)^2/(NO - NV)$.

Single-Crystal X-ray Analysis. A Nicolet P3/F automated four-circle diffractometer with a graphite monochromator was used for intensity data collection. All crystals exhibited satellite peaks in axial photographs due to crystal twinning. The crystal chosen for data collection had dimensions of 0.15 × 0.24 × 0.235 mm^3 and a large ratio of major-to-minor twin phases, as determined from the axial photographs. Experimental data collection and refinement parameters are given in Table 1. From the systematic absences, the space group could be either the centrosymmetric $P2_1/m$ or the noncentrosymmetric $P2_1$. The structure was solved by direct methods using MULTAN80.[6] Attempts to elucidate the structure in $P2_1/m$ symmetry were unsuccessful. However, using space group $P2_1$, the iron and bromine atoms were all located. The positions of the pyridinium ring atoms, excluding hydrogens, were found from Fourier syntheses. Computations were carried out with a modified version of the UCLA Crystallographic Program Package.[7] Since Br(9)–A(21) = 3.39(4) Å and Br(9)–A(22) = 3.43(4) Å distances are nearly identical, a disordered model was adopted in which the A(21) and A(22) sites are each half carbon and half nitrogen. An attempt to refine the pyridinium atoms anisotropically led to many nonpositive definite ellipsoids and a small observation-to-parameter ratio of ~6. Therefore, in the final cycles of least squares, iron and bromine atoms were refined

[⊗] Abstract published in *Advance ACS Abstracts*, June 15, 1994.

(1) (a) University of Illinois. (b) Argonne National Laboratory.
(2) Shaviv, R.; Lowe, C. B.; Zora, J. A.; Aakeröy, C. B.; Hitchcock, P. B.; Seddon, K. R.; Carlin, R. L. *Inorg. Chim. Acta* **1992**, *198*–200, 613.
(3) Ginsberg, A. P.; Robin, M. B. *Inorg. Chem.* **1963**, *2*, 817.
(4) Lowe, C. B.; Carlin, R. L.; Schultz, A. J.; Loong, C.-K. *Inorg. Chem.* **1990**, *29*, 3308.
(5) Zora, J. A.; Seddon, K. R.; Hitchcock, P. B.; Lowe, C. B.; Shum, D. P.; Carlin, R. L. *Inorg. Chem.* **1990**, *29*, 3302.
(6) Main, P.; Fiske, S. J.; Hull, S. E.; Lessinger, L.; Germain, G.; Declercq, J.-P.; Woolfson, M. M. MULTAN80. A System of Computer Programs for the Automated Solutions of Crystal Structures from X-Ray Diffraction Data. Universities of York, England, and Louvain, Belgium, 1980.
(7) Strouse, C. UCLA Crystallographic Program Package. University of California, Los Angeles, 1978.

0020-1669/94/1333-3051$04.50/0

Table 2. Atomic Positional and Thermal Parameters for $(pyH)_3Fe_2Br_9$

atom	x	y	z	U_{eq},[a] Å^2
Fe(1)	0.2702(7)	0.3244(7)	0.0640(4)	0.054(3)
Fe(2a)	0.2362(8)	0.2999(6)	0.5783(4)	0.056(3)
Br(1)	0.2621(7)	0.16827	0.0022(4)	0.075(2)
Br(2)	0.2703(7)	0.3078(6)	0.2340(4)	0.074(2)
Br(3)	0.5151(6)	0.4002(6)	0.0177(4)	0.079(2)
Br(4)	0.0242(6)	0.4055(6)	0.0056(4)	0.075(2)
Br(5)	0.2407(7)	0.3138(7)	0.7468(4)	0.078(2)
Br(6)	0.2606(8)	0.4455(4)	0.5129(4)	0.091(3)
Br(7)	-0.0229(7)	0.2217(6)	0.5248(4)	0.090(3)
Br(8)	0.4690(7)	0.2030(6)	0.5363(4)	0.073(2)
Br(9)	0.7482(7)	0.4580(6)	0.3414(3)	0.070(2)
N(1)	0.652(5)	0.054(2)	0.734(2)	0.067(10)*
C(11)	0.838(6)	0.053(4)	0.728(3)	0.084(15)*
C(12)	0.914(5)	0.124(3)	0.777(3)	0.067(13)*
C(13)	0.848(4)	0.185(2)	0.844(2)	0.032(9)*
C(14)	0.644(5)	0.181(3)	0.842(3)	0.049(11)*
C(15)	0.567(6)	0.116(3)	0.796(3)	0.069(13)*
A(21)[b]	0.794(5)	0.528(4)	0.579(3)	0.090(14)*
A(22)[b]	0.753(4)	0.441(3)	0.590(3)	0.053(10)*
C(21)	0.718(6)	0.392(4)	0.679(4)	0.099(17)*
C(22)	0.749(6)	0.453(3)	0.767(3)	0.072(14)*
C(23)	0.790(6)	0.536(4)	0.757(4)	0.090(17)*
C(24)	0.806(7)	0.584(4)	0.657(4)	0.113(19)*
N(3)	0.734(4)	0.244(3)	0.273(3)	0.075(11)*
C(31)	0.787(7)	0.265(4)	0.188(4)	0.102(19)*
C(32)	0.794(8)	0.203(5)	0.128(4)	0.119(21)*
C(33)	0.766(7)	0.109(4)	0.139(4)	0.091(17)*
C(34)	0.689(8)	0.085(4)	0.231(4)	0.118(21)*
C(35)	0.675(7)	0.153(4)	0.300(4)	0.104(18)*

[a] Values with an asterisk are for atoms refined isotropically. For atoms refined anisotropically, $U_{iso} = {}^1/_3\Sigma_i\Sigma_j U_{ij}a_i^*a_j^*\mathbf{a}_i\mathbf{a}_j$. [b] Half carbon and half nitrogen atoms.

Table 3. Interatomic Distances (Å) and Angles (deg) in $(pyH)_3Fe_2Br_9$

Fe–Br Distances and Angles			
Fe(1)–Br(1)	2.379(9)	Fe(2)–Br(5)	2.318(8)
Fe(1)–Br(2)	2.346(8)	Fe(2)–Br(6)	2.271(9)
Fe(1)–Br(3)	2.285(7)	Fe(2)–Br(7)	2.354(9)
Fe(1)–Br(4)	2.311(8)	Fe(2)–Br(8)	2.352(8)
Br(1)–Fe(1)–Br(2)	105.0(3)	Br(5)–Fe(2)–Br(6)	108.7(4)
Br(1)–Fe(1)–Br(3)	110.2(3)	Br(5)–Fe(2)–Br(7)	108.3(3)
Br(1)–Fe(1)–Br(4)	109.9(3)	Br(5)–Fe(2)–Br(8)	109.1(3)
Br(2)–Fe(1)–Br(3)	111.9(3)	Br(6)–Fe(2)–Br(7)	113.3(4)
Br(2)–Fe(1)–Br(4)	110.3(3)	Br(6)–Fe(2)–Br(8)	110.9(3)
Br(3)–Fe(1)–Br(4)	109.5(3)	Br(7)–Fe(2)–Br(8)	106.4(3)
Br(9)···Pyridinium Hydrogen Bond Distances			
Br(9)···N(3)	3.18(4)	Br(9)···A(21)[a]	3.40(5)
Br(9)···A(22)[a]	3.42(4)	Br(9)···N(1)	3.46(3)
Br···Br Contacts (<4.5 Å) in Ascending Order			
Br(3)···Br(4)	3.912(8)	Br(2)···Br(6)	4.305(7)
Br(7)···Br(8)	3.912(8)	Br(1)···Br(4)	4.335(8)
Br(1)···Br(5)	4.067(8)	Br(3)···Br(5)	4.339(8)
Br(1)···Br(3)	4.196(8)	Br(6)···Br(7)	4.351(9)
Br(4)···Br(5)	4.216(7)	Br(2)···Br(9)	4.415(8)
Br(8)···Br(9)	4.252(7)	Br(6)···Br(9)	4.457(8)
Br(6)···Br(8)	4.284(8)	Br(7)···Br(9)	4.494(8)

[a] Disordered half carbon, half nitrogen atoms.

anisotropically and all pyridinium atoms were refined isotropically. Final atomic positional and thermal parameters are presented in Table 2, and interatomic distances and angles are given in Table 3. Atom labels and thermal ellipsoids are shown in Figures 1 and 2.

The magnetic susceptibility was measured by the usual low-frequency, ac zero-field method. The specific heat of a polycrystalline sample was measured in a recently described calorimeter.[8]

Results and Discussion

Crystal Structure. The structure of $(pyH)_3Fe_2Br_9$ is confirmed as containing $[FeBr_4]^-$ ions, along with pyridinium cations and an uncoordinated Br^- anion. Even so, it is not isostructural with its chloride analog[2] and belongs to a different crystal class. The Fe–Br bond lengths range from Fe(2)–Br(6) = 2.271(9) Å to Fe(1)–Br(1) = 2.379(9) Å for the two different slightly distorted tetrahedral units. Angles within the anions range from 105.0(3) to 113.3(4)°, with an overall average of 109.5°. Within the pyridinium rings, bond lengths and angles are variable, and the thermal parameters for these atoms are dissimilar as well. Therefore, some localized disorder seems evident within the ring structures.

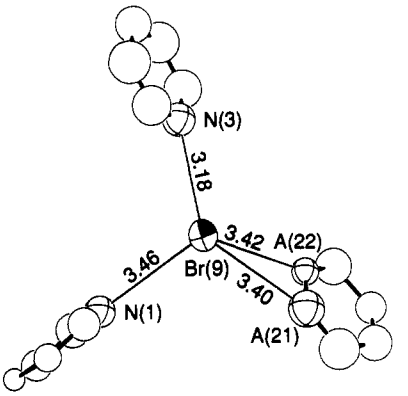

Figure 1. Hydrogen bonds between the Br(9) anion and the pyridinium cations. Atoms A(21) and A(22) were refined as disordered half carbon, half nitrogen atoms. All atoms are drawn at the 50% probability level.

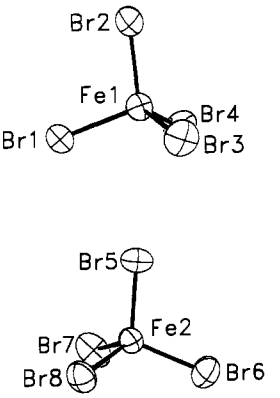

Figure 2. The two crystallographically independent $[FeCl_4]^-$ anions plotted in their relative positions in the unit cell. The *b* axis is horizontal, and the *c* axis is vertical. All atoms are drawn at the 50% probability level.

Short N–H···Br(9) hydrogen bond contacts are seen between the three nitrogen-coordinated hydrogens and the free bromide ion. These are given in Table 3 for the illustration in Figure 1. The entire unit cell is pictured in Figure 2. With two molecules per unit cell, the iron tetrahedra are aligned with one of their pseudo-3-fold axes nearly parallel to the crystallographic *c* axis. A view down this axis reveals the staggered conformation of the basal bromides. The pyridinium rings separate the tetrahedra mostly along the *b* direction. Consequently, the longest unit length for the cell is *b*, in order to accommodate the large pyridinium cations.

A detailed look at the structure for possible superexchange pathways requires a comparison of close Br···Br distances of less than 4.5 Å as given in Table 3. The next-shortest distances are all greater than 5.0 Å. The Fe–Br···Br–Fe pathways along the *a* axis are shortest but not extremely shorter than some of those along *c* which involve the bromines Br(2) and Br(5) or those remaining which zigzag in the *a*–*b* plane. Figure 3 illustrates the various contacts between tetrahedra and the associated numbering scheme of the atoms. Since the ring structures are not bound to any Fe atom and do not cause large separations between layers of metal ions, lower dimensional magnetic behavior due to poor superexchange paths along one or more directions is not expected.

(8) Shaviv, R.; Merabet, K. E.; Shum, D. P.; Lowe, C. B.; Gonzalez, D.; Burriel, R.; Carlin, R. L. *Inorg. Chem.* **1992**, *31*, 1724.

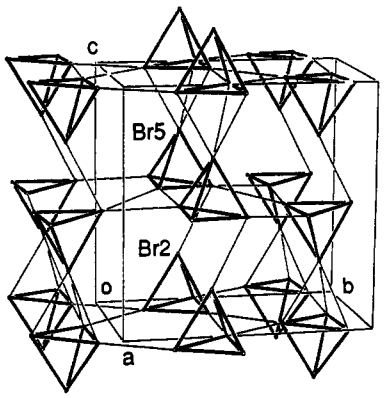

Figure 3. Fe–Br···Br–Fe contacts of less than 4.5 Å. The $[FeBr_4]^-$ anions are shown as Br_4 tetrahedra without the Fe atom. Note the dimerization along the *c* axis.

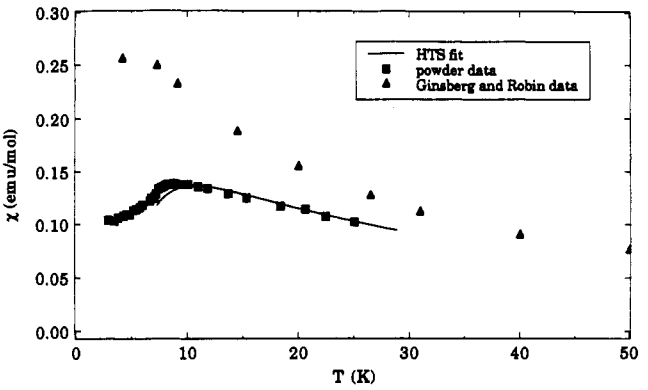

Figure 4. Powder susceptibility measurement between 2 and 30 K for $(pyH)_3Fe_2Br_9$. The data of Ginsberg and Robin[3] are shown for comparison. The solid line is the sc Heisenberg high-temperature series equation described in the text with $g = 1.98$ and $J/k_B = -0.43$ K.

Magnetic Susceptibility. Magnetic susceptibility measurements were made over the temperature range 1.1–30 K. Problems were encountered due to the fragility of the crystals, which had a tendency to crack as they were cooled. Cracked crystal fragments would separate and reorient or even shatter, leading to lost material during measurement, and thus caused difficulty in scaling the susceptibility. Measurements were made on uniformly ground powders in closed sample holders and scaled without difficulty. Unfortunately, this limits the amount of information which might be obtained from single-crystal measurements. Crystal measurements were also made and scaled using CMN to arbitrary units, but it proved troublesome to determine the percentage and orientation of twinning in the crystals. These data, for measurements in which the measuring field is applied along two perpendicular directions through the crystal, show that the magnetic behavior of the material is roughly typical of an antiferromagnet below T_c. No out-of-phase component for the susceptibility was observed, and thus this material possesses either hidden or no canting between its sublattices. Antisymmetric exchange coupling, if present, would be allowed by symmetry[9] along the *a* direction of the crystal perpendicular to a mirror plane which bisects the Fe(1) and Fe(2) tetrahedra parallel to the *b* axis. We emphasize these points because canting is so prevalent with the other compounds in this series.

A comparison of the powder data of this study and those of Ginsberg and Robin for $(pyH)_3Fe_2Br_9$ is shown in Figure 4. It is clear from the data shown that these are not the same materials. The data of Ginsberg and Robin rise much more steeply, with some sort of inflection point in the data at lower temperatures. Our data exhibit a susceptibility maximum at 8.78 K of $\chi_{max} = 0.139$ emu mol^{-1}. We speculate from the similarity of chemical analysis yet very different susceptibility results that there may be two forms of the compound with this stoichiometry.

Table 4. Values of the Exchange parameter, J/k_B, for Tetrabromoferrates(III)

source	$(pyH)_3Fe_2Br_9$[a]	$[4\text{-Cl(py)H}]_3Fe_2Br_9$[b]
HTS fit, K	−0.43	−0.47
χ_{max}, K	−0.42	−0.45
$T(\chi_{max})$, K	−0.33	−0.33
T_c, K	−0.30	−0.32

[a] This work. [b] Reference 2.

The solid curve shown in Figure 4 is a comparison of the 2[(py)H][$FeBr_4$]·[(py)H]Br data to the HTS expansion of $1/\chi$ for the $S = {}^5/_2$ three-dimensional Heisenberg model antiferromagnet with a sc lattice[10] with $g = 1.98$ and $J/k_B = -0.43$ K. This value of J/k_B is a factor of 5 larger than the exchange constant determined for the chloride compound described in the previous paper.[2] The data compare well to those of the model. Three-dimensional order is seen, from the greatest slope in the data, to occur at 7.4 ± 0.2 K. In the same way, a fit was made to the data of Ginsberg and Robin down to 7.3 K, which gave $g = 2.00$ and $J/k_B = -0.235$ K. However, due to the infrequency of data at lower temperatures, the inflection is not characterized. From close scrutiny to the interactions shown in Figure 3 for our $(pyH)_3Fe_2Br_9$ sample, arguments could be made in favor of a distorted body-centered-cubic lattice with eight approximate nearest neighbors. The eight nearest Fe neighbors to Fe(1) range from 6.6 to 8.4 Å, and nearest Fe---Fe distances from Fe(2) extend from 6.6 to 8.5 Å. The data, when analyzed using a HTS expansion for a bcc lattice with coefficients previously given,[11] could not be fit well with reasonable parameters to sufficiently low temperatures. The variation in Fe---Fe distance is probably the reason for this, since exchange falls off severely with distance when appropriate bridging ligands are not present.

Estimates of the exchange interaction by various means may be compared in order to evaluate the correctness of the model for the magnetic behavior of $(pyH)_3Fe_2Br_9$. The parameter J/k_B is calculated from the values of T_c, $T(\chi_{max})$, and χ_{max} obtained from the data using the relations found in ref 2. Values obtained in this manner for our data are given in Table 4. These are in substantial agreement with the simple cubic model behavior, at least to a first approximation.

The overall strength and type of superexchange interactions in 2[(py)H][$FeBr_4$]·[(py)H]Br are very similar to those seen for 2[4-Cl(py)H][$FeBr_4$]·[4-Cl(py)H] Br (as compared in Table 4), despite the difference in space group and cell size. The slightly lower T_c value follows the trend between 2[(py)H][$FeCl_4$]·[(py)H]-Cl and 2[4-Cl(py)H][$FeCl_4$]·[4-Cl(py)H]Cl, and stronger interactions are found for the bromides. The absence of canting, or a much reduced magnitude in the case of the chloride, seems to be a result of the difference in structure for the pyridinium-containing compounds.

Specific Heat Measurements. The specific heat of the title compound is reported in Figure 5, along with the estimated lattice contribution; the latter was derived by a procedure described earlier in detail.[8] An odd-shaped, double-peaked λ feature, with maxima at 7.3 and 8 K, is observed. The lower temperature peak is consistent with the susceptibility data, reflecting the onset of long-range order at 7.3 K. There is no evidence in the susceptibility measurements however for any transition at the higher temperature of 8 K. The peaks are not as distinct nor as well-separated as are the two λ peaks observed for $[4\text{-Cl(py)H}]_3Fe_2Br_9$, at 5.50

(9) Moriya, T. Weak Ferromagnetism. In *Magnetism*; eds. Rado, G. T., Suhl, H., Eds.; Academic Press: New York, London, 1963; Vol. 1, pp 93–6.

(10) de Jongh, L. J.; Breed, D. J. *Solid State Commun.* **1974**, *15*, 1061.
(11) Rushbrooke, G. S.; Wood, P. J. *Mol. Phys.* **1958**, *1*, 257.

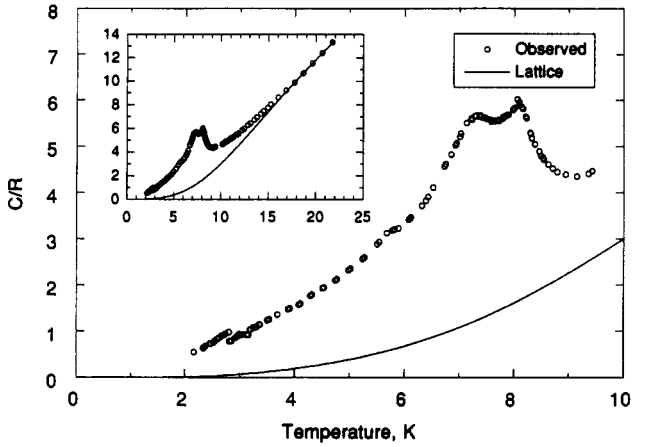

Figure 5. Specific heat of $(pyH)_3Fe_2Br_9$. The circles are the measured data points, and the solid curve is the calculated lattice specific heat.

and 7.92 K.[12] Again, there was no evidence with that compound in the susceptibility data for any transition at the higher temperature either. On the other hand, $[4\text{-}Cl(py)H]_3Fe_2Br_9$ exhibited canting while 2[(py)H][FeBr4]·[(py)H]Br does not.

(12) Shaviv, R.; Lowe, C. B.; Carlin, R. L. *Inorg. Chem.* **1993**, *32*, 1543.

A small discontinuity appears in the data at about 2.2 K. It could signify a long-range order transition, but there is so little entropy associated with this feature that most of the measured specific heat would have to be attributed to short-ranged order. There is however no evidence for this either in the susceptibility or in the structure. At this time we can best assign it as an experimental artifact.

Acknowledgment. This work was supported by the Solid State Chemistry Program of the Division of Materials Research of the National Science Foundation, under Grants DMR-8515224 and DMR-8815798. Acknowledgment is made to the donors of the Petroleum Research Fund, administered by the American Chemical Society, for partial support of this research. Work at Argonne National Laboratory was sponsored by the U.S. Department of Energy, Office of Basic Energy Sciences, Division of Materials Sciences, under Contract W-31-109-Eng-38.

Supplementary Material Available: Figure S1, showing a stereoview of the unit cell, Table S1, listing anisotropic thermal parameters, and Table S2, giving interatomic distances and angles (7 pages). Ordering information is given on any current masthead page.